Arabian Journal of Geosciences (2020) 13: 925
https://doi.org/10.1007/s12517-020-05884-9

ORIGINAL PAPER

Elemental and isotopic geochemistry of carbonate rocks from the Pila Spi Formation (Middle–Late Eocene), Kurdistan Region, Northern Iraq: implication for depositional environment

Faraj Habeeb Tobia[1] · Hikmat Safi Al-Jaleel[1] · Awaz Kareem Rasul[1]

Received: 9 April 2020 / Accepted: 20 August 2020 / Published online: 9 September 2020

Abstract

Major, trace, rare earth elements (REE), and stable isotopic compositions in carbonate rocks of Pila Spi Formation were measured to constrain the source of rare earth elements and depositional environment. The low ΣREE content (average = 6.53 ppm, $n = 14$) indicates that the carbonates seawater-like REE patterns with (1) LREE depletion (average $(Nd/Yb)_n$ = 0.81), (2) HREE enrichment, (3) negative Ce anomaly (average = 0.91), and (4) superchondritic Y/Ho ratio (average = 30.07); slightly lower average value of Y/Ho ratio than the typical seawater value (~ 44–74) suggests modification of the seawater by input of fresh water. The $(Nd/Yb)_n$ and $(Dy/Yb)_n$ ratios of the Pila Spi carbonates have similarity with that of the Arabian sea carbonate. The low concentrations of U (0.35–1.0 ppm) suggest the deposition under oxygen-rich environment. This study indicates that the carbonates still preserve their original seawater-like REE pattern, provided that the contamination with terrigenous materials was small, and they serve as a seawater proxy. The Pila Spi carbonates have $\delta^{13}C$ values ranged from − 6.17 to 0.76‰ PDB, and the $\delta^{18}O$ values range between − 3.85 and 0.46‰ PDB. The positive correlation between $\delta^{13}C$ and $\delta^{18}O$ ($r = 0.949$, $n = 14$) values indicates the alteration of original isotopic compositions due to diagenesis. Finally, it is conceived that the Pila Spi carbonate was deposited in the lagoon environment with seawater invading and mixing of the continental (terrigenous) materials to the basin is viable.

Keywords : Stable isotope · Carbonate rocks · Eocene · Northern Iraq · Provenance

Introduction

Depositional environment of the carbonate rocks can be depicted by chemical, physical, and biological parameters. The major and trace elements provide knowledge about the overall composition of the carbonate rocks and their depositional conditions (Srivastava and Singh 2017). Furthermore, rare earth elements (REE) patterns are mainly influenced by depositional environment (Murray et al. 1992; Madhavaraju and Ramasamy 1999) and diagenetic processes (Schieber 1988; Armstrong-Altrin et al. 2003; Morad et al. 2010; Tobia 2018). Also, REEs are regarded as an indicator to depositional environment such as marine anoxia (German and Elderfield 1990; Murray et al. 1991), palaeooceanic redox conditions (Elderfield and Pagett 1986; Liu et al. 1988; Jones and Manning 1994; Kato et al. 2002; Pattan et al. 2005; Deepulal et al. 2012; Tobia and Shangola 2016; Patra and Singh 2017), and variations in surface productivity (Toyoda et al. 1990). The distribution and employment of the REEs in carbonate rocks and marine waters have been discussed by several researchers (Piper 1974; Elderfield et al. 1990; Webb and Kamber 2000; Armstrong-Altrin et al. 2003; Nothdurft et al. 2004; Alexander et al. 2008; Madhavaraju et al. 2010; Nagarajan et al. 2011).

Stable isotope (oxygen and carbon) signatures of carbonates have been used to provide information on climatic and environmental conditions (Tanner 2009). The nature of the depositional environment and diagenesis may influence the

Responsible Editor: Domenico M. Doronzo

✉ Faraj Habeeb Tobia
farajabba58@gmail.com; faraj.tobia@su.edu.krd

Hikmat Safi Al-Jaleel
hikmatsafi@gmail.com

Awaz Kareem Rasul
awaz.rasul@su.edu.krd

[1] Department of Geology, Salahaddin University, Erbil, Kurdistan Region, Iraq

stable isotopic values (Talbot 1990; Tandon and Andrews 2001; Cuna et al. 2001; Tobia 2018).

Geochemistry of carbonate rocks is commonly used to illustrate the controlling factors that are responsible for the character of carbonate sediments during and after the deposition (Armstrong-Altrin et al. 2011; Nagarajan et al. 2011; Tobia 2018). Furthermore, detrital input and paleo-redox conditions can be recognized through the geochemical study of the carbonate rocks (Armstrong-Altrin et al. 2003; Fu et al. 2011; Hua et al. 2013).

Previous works within the Middle-Late Eocene Pila Spi Formation are mainly focused on the lithofacies aspects and suggest their deposition in a marine environment rather than lagoon (Khanaqa 2011; Al-Mashaikie and Latif 2017), and the influence of the dolomitizatoin on the reservoir characteristics (Othman and Al-Qayim 2010). There is a limited study on geochemistry of the Pila Spi Formation from selected sections in Northern Iraq (Kadhim and Hussein 2016). Therefore, a systematic, detailed work emphasis on geochemical aspects of Pila Spi carbonate is required to strengthen the knowledge not only on depositional environment within the Middle-Late Eocene but also for deciphering paleo-redox condition, detrital input, and seawater chemistry during deposition of Pila Spi carbonate.

Several studies refer that the formation was deposited in shallow lagoonal setting (e.g., Jassim and Goff 2006), while Al-Sakry (1999) believed that the formation was deposited in a shelf and shallow lagoonal environment. Othman and Al-Qayim (2010) subdivided the Pila Spi Formation in Taq Taq oil field and Haibat Sultan Mountain into four lithologic units from bottom to top: lower brecciated and silicified unit, dolomitized tidal flat limestone, lagoonal limestone, and dolostone and upper brecciated dolomitic limestone. Also, Khanaqa (2011) interpreted new facies in Pila Spi Formation at Sulaimanyia, NE, Iraq, such as massive and high fossil contents of algae, corals, bryozoans, and bioclasts; also floatstone, bindstone, framstones, bafflestones, and rudstone microfacies have been identified; these facies revealed new environmental and paleogeographic setting for the Middle-Late Eocene in NE Iraq, which is a carbonate ramp with low topographic patchy reef, back reef, and lagoon.

The present study aimed to better understand the geochemical characteristics and palaeo-environment of Pila Spi carbonates during the Middle-Late Eocene time period, based on the major, trace, rare earth elements, and stable isotope geochemistry.

Geological setting

The indication for subduction and the final closure of neo-Tethys Ocean is supplied by calc-alkaline basic and intermediate volcanic rocks of Paleocene-Eocene age which have been depicted in NE Iraq (Fig. 1). These rocks formed in back arc or in island arc rifts. These volcanic rocks formed in active margin setting close to the Arabian Plate (Jassim and Goff 2006). During the subduction, two pulses of uplift in Paleocene and Eocene age occurred along the NE margin of the Arabian Plate.

The Megasequence AP10 (Middle Paleocene-Eocene) was recognized; the renewed subduction and volcanic arc activity were associated with the final closure of neo-Tethys Ocean. This led to uplift along the NE margin of the Arabian Plate with the formation of basins and ridges.

Ditmar and the Iraqi-Soviet Team (1971) suggested regional unconformity at the base of the Middle Eocene. The Megasequence AP10 was divided for two sequences: Paleocene-Early Eocene and Middle-Late Eocene sequences. The latter was deposited to the SW of an emergent uplift. The Gercus Red Beds were deposited at narrow basin between the uplifted area in the NE and a ridge located along the NE side of Balambo-Tanjero Zone. At the end of the Mid Eocene, the clastic sediments provide from the uplifted area to the NE and the basin was filled with lagoonal carbonates of Pila Spi Formation.

The formation was first described by Lees in 1930 from the Pila Spi area of the High Folded Zone, and redefined by Wetzel in 1947 and amended by Bellen et al. (1959). The type section was drawn under the water of Darbandi Khan Dam; thus, the supplementary type section was described at Kashati on the Barand Dagh about 10 km to the north of Darbandi Khan Town.

Further northeastwards older strata of Paleogene units were exposed, forming the hard prominent ridge of the Haibat Sultan Mountain, which extends in NW-SE trend, and representing the southwestern limb of Bana Bawi anticline. This ridge is geomorphological high with 1047 m elevation (a.s.l.), where the hard limestone beds of the Pila Spi Formation formed the weathering-resistant crestal part of the ridge. The lower part of the formation comprises well bedded, hard, porous, bituminous, white, poorly fossiliferous limestones. The upper part consist well bedded, bituminous, chalky, and crystalline limestones with bands of white chalky marl and with chert nodules towards the top. Fossils are abundant and refer to a Late Eocene, and may be partly of Middle Eocene age in North Iraq. The lower boundary of the Pila Spi Formation appears to be conformable and gradational in the type section in NE Iraq, where it overlies the Gercus Formation. The boundary is either interfingering, as in Bekhme area (Al-Qayim and Al-Shaibani 1997), or marked by locally distributed (0.5–1 m thick) conglomerate horizon, and as in Shaqlawa area (Al-Qayim et al. 1994), and Haibat Sultan Mountain (Al-Qayim et al. 1988). The upper boundary is unconformable with the overlying rocks are

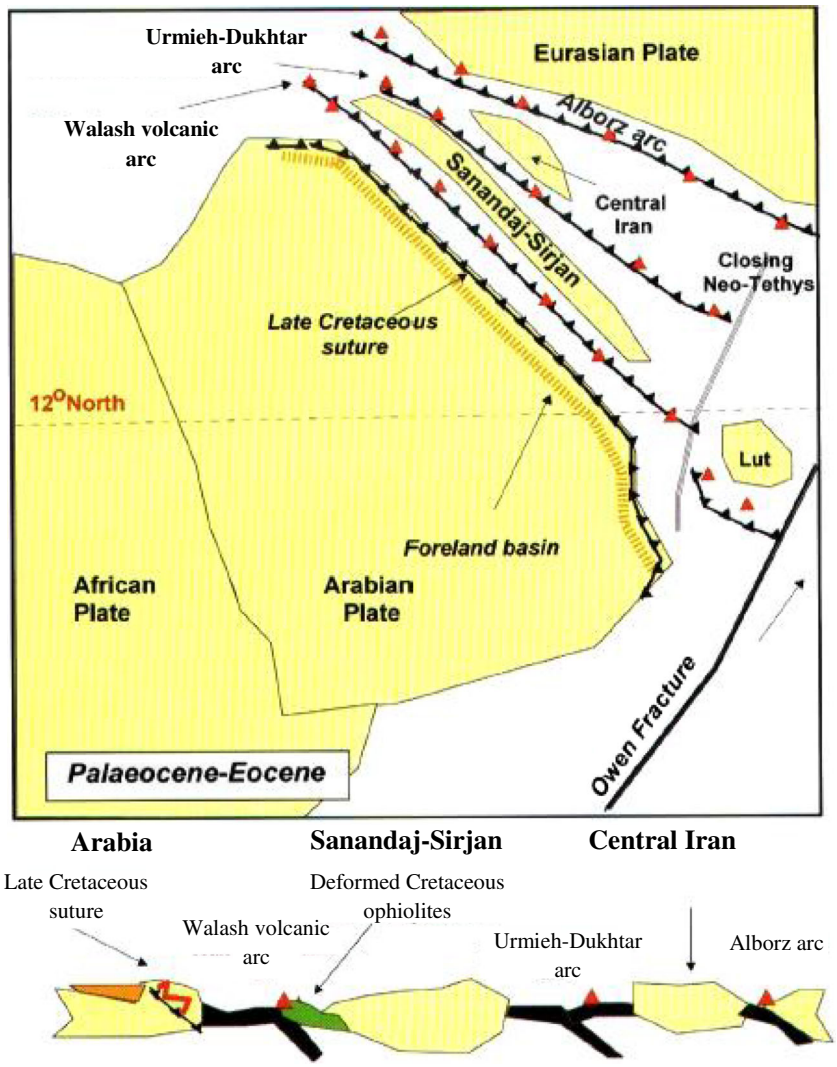

Fig. 1 Paleocene-Eocene geodynamic development of the Arabian Plate (Jassim and Goff 2006)

mostly of Miocene age (e.g., Fatha Formation). Kadhim and Hussein (2016) stated that Pila Spi limestone is commonly of mudstone and few beds of wackestone and mostly affected by the dolomitizatoin and diagenetic processes, and they suggest the shallow environment with low salinity due to the low Sr.

Methodology

Two surface sections were selected, the first at Haibat Sultan Mountain (70 m thick), which is about 3 km to the northeast of the Quwaisanjaq Ciy at 36° 04′ 55″ N and 44° 39′ 56″ E (Fig. 2), and the second near Bekhme Village (26 m thick) at 36° 39′ 36″ N and 44° 13′ 48″ E (Fig. 3). The Pila Spi Formation is completely exposed at the ridges with accessible and road cut outcrops. Selected fourteen samples (9 samples from Haibat Sultan and 5 samples from the Bekhme area; Figs. 2 and 3) were thin-sectioned and occasionally treated with Alizarin Red solusion (Dickson 1965) to investigate their petrographic components and texture using polarized microscope. A detailed petrographic study covering more than 30 thin sections was carried out.

The chemical analysis of major elements (Al, Ca, Fe, K, Mg, Na, and S) was carried out by inductively coupled plasma–atomic emission spectrometry (ICP-AES) after fuse bead and acid digestion (ME-ICP06 code) except Si was determined by gravemetric method (Matilainen and Tummavuori 1999). One gram of sample was heated to 1000 °C in porcelain crucibles for 1 h to measure the loss on ignition (LOI). The analysis of trace elements (Ti, Co, Cr, Cu, Mn, Mo, Nb, Ni, P, Rb, Sc, Sr, U, V, Y, Zn, and Zr) and rare earth elements (La, Ce, Pr, Nd, Sm, Eu, Gd, Tb, Dy, Er, Ho, Tm, Yb, and Lu) were carried out by inductively coupled plasma–mass spectrometry (ICP-MS) after four acid digestion (ME-MS61r code) at the ALS international laboratory in Spain. Internationally

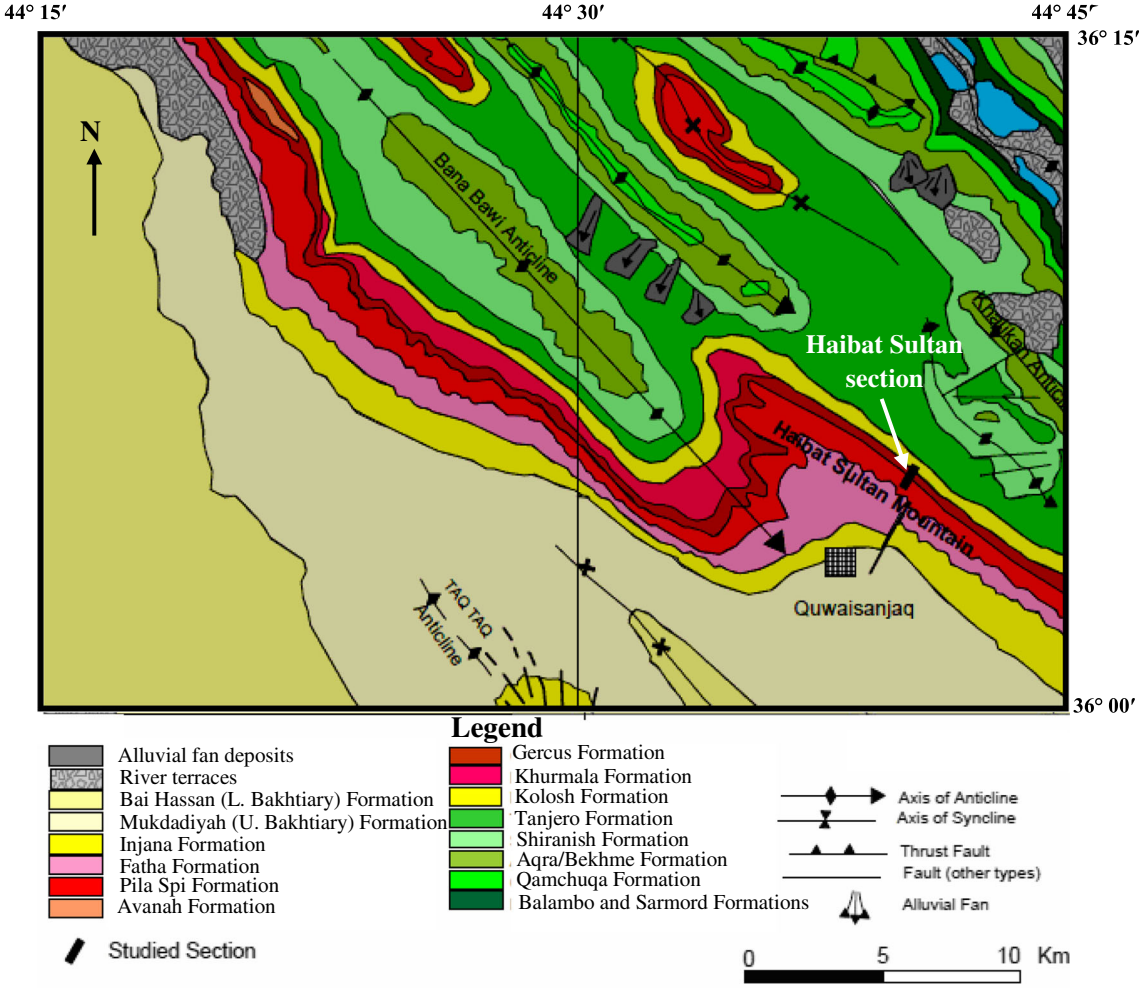

Fig. 2 Geological map for the studied area at Haibat Sultan section (Sissakian 1997)

recognized standard materials GBM908-10 and MRGeo08 were used as references. The analytical accuracy ranges from 2 to 10%, and precision varies from 1 to 8%. The REE ratios are compared with that of shallow and deep water marine carbonates. The REE concentrations are normalized to PAAS (Taylor and McLennan 1985).

The $^{13}C/^{12}C$ and $^{18}O/^{16}O$ isotopic ratios were determined at the Stable Isotope Laboratory of the Cornell University, USA. For C- and O-isotopic determinations, powdered samples were treated with H_3PO_4 at 25 °C for 3 days to release CO_2. The released gas was measured for ^{13}C and ^{18}O by mass spectrometry, using the reference gas BSC (Borborema Skarn Calcite) calibrated against NBS-18 that has a value of − 23.20% and − 5.01%, respectively, and for NBS-19 have − 2.20% and 1.95%, respectively. The isotopic results for both C and O are reported as per mil (‰) notation relative to Vienna Pee Dee Belemnite (V-PDB). The uncertainties of the isotope were 0.03‰ for C and 0.06‰ for O, founded on multiple analyses of standard dolomite.

Results

Petrography

The studied Pila Spi carbonates have different degree of diagenetic effects, especially, dolomitization, which obliterate most of the original rock texture. Most of the examined samples belong to either dolomitic limestone or dolostone, due to intensive dolomitization process, which affect the Pila Spi carbonate and destroyed partly to completely the original fabric of the rock. Dolomite microfacies are the dominant in the studied carbonate. According to the crystal size and crystal boundary shape, Sibley and Gregg (1987) and Lucia (2007) classified the dolomite fabric to different microfacies.

Three types of dolomite were distinguished: unimodal fine crystalline planar-e to planar-s dolomite, which planar-e dolomite has straight and planar crystal boundaries (Fig. 4a), and the crystals tend to be euhedral, and for planar-s dolomite the crystals are subhedral (Sibley and Gregg 1987); it is an early

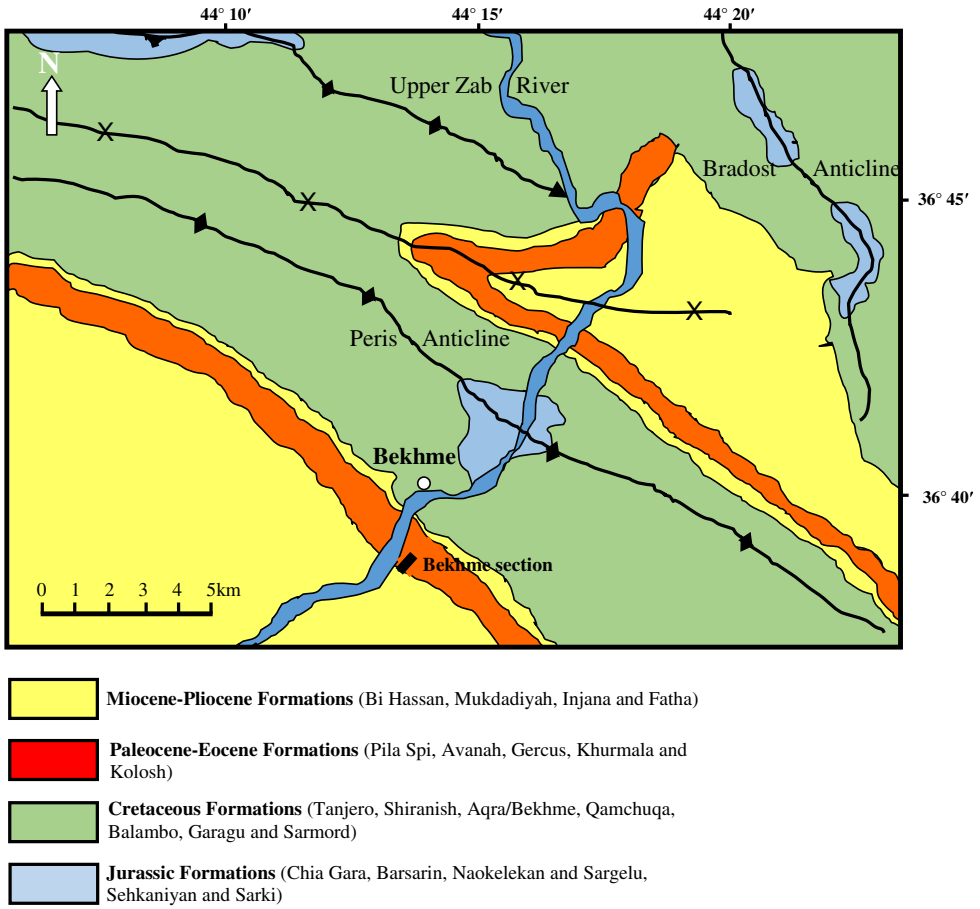

Fig. 3 Geological map for the studied area at Bekhme section (Sissakian 2000)

diagenetic dolomite. Porosity type associated with this microfacies includes fenestral, vuggy, and moldic, (Fig. 4a, b, c). The second type is unimodal fine crystalline planar-s to non-planar-a dolomite. The texture is represented by subhedral and closely packed anhedral crystals, with mostly curved boundaries (Fig. 4b). It is distributed within the most of the studied intervals of the Pila Spi Formation. Good amount of porosity seems to be related to this microfacies especially micro-vugs. The last type is bimodal fine to medium crystalline planar-s to non-planar-a dolomite with the amount of moldic and micro-vugs porosity (Fig. 4d, f, g). This type of dolomite is characterized by mixed distribution of crystal size of fine and medium crystalline mosaic. The finer parts are anhedral to subhedral crystal shape, and the medium size crystals are commonly euhedral to subhedral. Bimodal term refers to heterogeneous crystal sizes of dolomite (Gregg and Sibley 1984). This microfacies might be developed by intensive dolomitization of a limestone with originally bioclastic packstone type (Randazzo and Zachose 1984). Ghosts of original skeletal fragments indicate that the original depositional microfacies type of this dolostone is seemingly associated with foraminiferal-bioclastic wackestone (Fig. 6d). However, silicification of late diagenetic stages also present a common feature in a studied sections as euhedral quartz crystals and microquartz (Fig. 4e). Microstylolite and iron oxides are observed in the studied rocks especially in the last type of microfacies (Fig. 4f, g). Also, blocky calcite cement of late diagenesis was recorded (Fig. 4h). This description is largely confirming with that of Othman and Al-Qayim (2010), and they conclude the massive hard dolostone bed, restored original fabric, and components and indicate deposition in a sheltered lagoonal environment prevailed for a long and relatively stable period.

Many types of porosity were observed: Fenestral porosity (Fig. 4a), commonly associated with stromatolitic dolomite facies and the pores, is normally much larger than the grain size (Major et al. 1990). It is a primary porosity bound to syn-sedimentary open-space structures, and commonly associated with supratidal and intertidal, algal-, and microbial-related, mud-dominated sediments (Choquette and Pray 1970; Lucia 2007). Vuggy porosity (Fig. 4b) is secondary solution pores that are not fabric selective; i.e., the pores cut across grains and/or cement boundaries (Choquette and Pray 1970). Vugs are commonly started as moldic or intercrystalline pores and enlarged by further solution a diagenetic modification into larger and irregular cavities (Lucia 2007). Moldic porosity

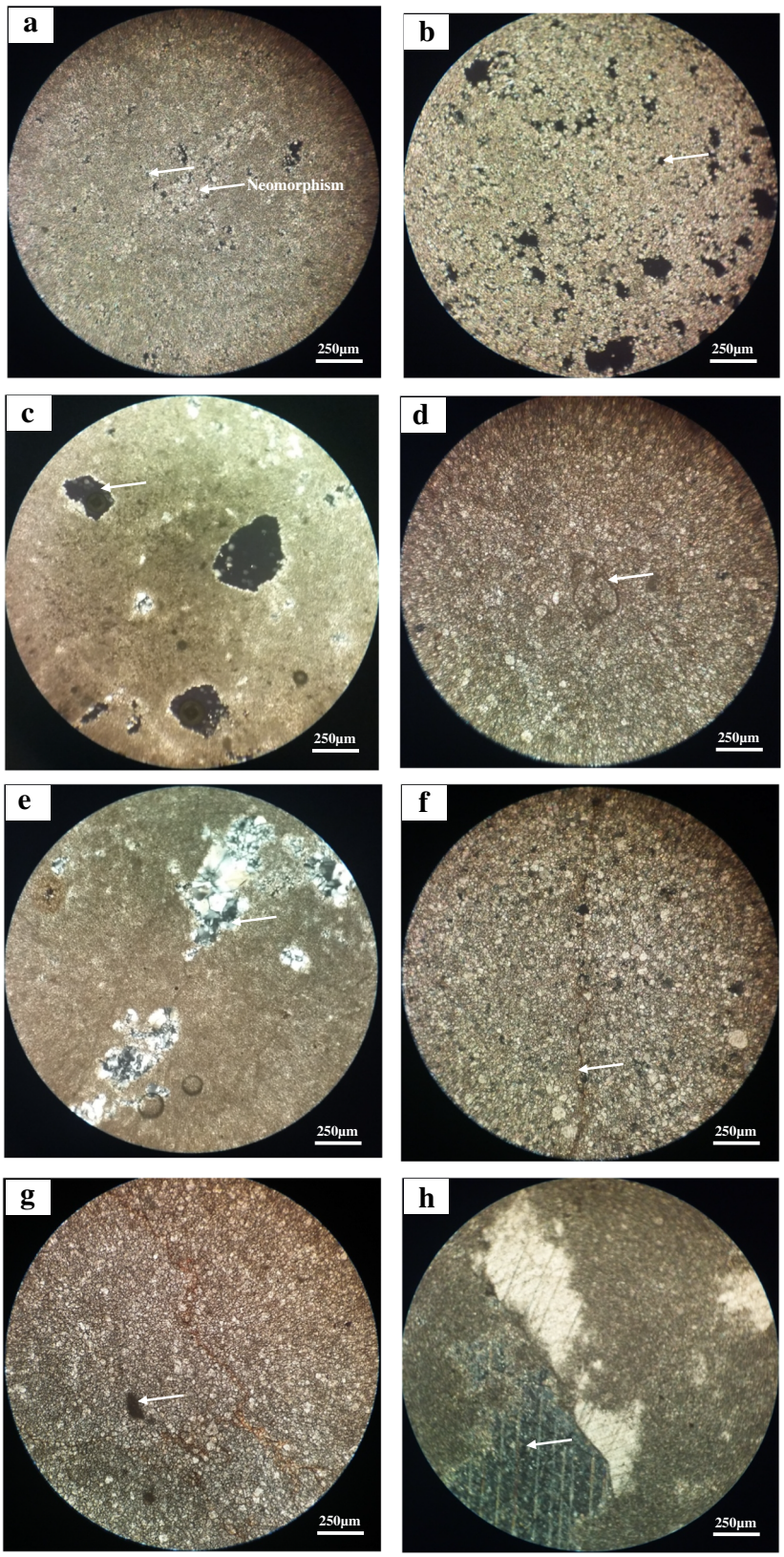

Fig. 4 Microphotographs for Pila Spi carbonates: **a** Fenestral porosity in unimodal fine crystalline planar-e dolomite, Haibat Sultan section. **b** Vuggy porosity in fine crystalline planar-s to nonplanar-a dolomite. **c** Moldic porosity in unimodal fine crystalline planar-e dolomite. **d** Mimic foraminifera in bimodal fine to medium crystalline planar-s to non-planar-a dolomite. **e** Siliceous cement filling inter-crystalline porosity of a fine crystalline dolomite. **f** Microstylolite in fine to medium dolomite. **g** Iron oxide grains in fine to medium dolomite. **h** blocky calcite cement of late diagenesis. All microphotographs are under XN

(Fig. 4c) is secondary pore that forms by selective, complete, or partial dissolution of carbonate grain; this definition is slightly modified by Lonoy (2006) that includes pores formed by partial dissolution and recrystallization.

Major elements

The major oxide contents are given in Table 1, and the Post-Archaean Australian Shale (PAAS)–normalized oxides of the Pila Spi carbonate are represented in Fig. 5. CaO is the dominant oxide in the studied rocks it ranges from 25.97 to 44.52% with an average 29.15%. MgO is the second dominant oxide of moderate variation (6.27 to 21.41 %) with an average 18.79%. Low content of Al_2O_3 is observed in the studied samples (0.4 to 1.73%, average 0.90%). The average contents of Na_2O, K_2O, MnO, TiO_2, and P_2O_5 (0.08, 0.05, 0.019, 0.015, and 0.01; respectively) are very low in the carbonate samples (Table 1). The dolomitization ratio proposed by Singh et al. (2013) ranges from 0.141 to 0.774 in the studied carbonates.

CaO shows significant positive correlation with TiO_2, Al_2O_3, SO_3, and P_2O_5 and a negative correlation with MgO and Na_2O, while MgO records negative correlation with TiO_2, Al_2O_3, SO_3, and P_2O_5 and positive with Na_2O (Table 2). Significant positive correlation was observed between Al_2O_3 and other major oxides (TiO_2, Fe_2O_3, CaO, K_2O, SO_3) and negative with MgO and MnO. Most of major elements (except MgO) show positive correlations with TiO_2 (Table 2).

Trace elements

The trace element concentrations of the Pila Spi carbonates are listed in Table 1, and the PAAS normalized trace element values (Taylor and McLennan 1985) are presented in a spider diagram (Fig. 5). Large variations are recorded in the concentration of Cr, Cu, Zr, and Mo, and least variation are shown in Rb, Sr, U, Y, Nb, Sc, Co, Ni, and Zn (Table 1). The Rb ranges from 0.4 to 2.0 ppm in these carbonates (Table 1). The Sr ranging from 78.4 to 211 ppm is much lower than the average value of the PAAS (200 ppm) and lithospheric carbonate (610 ppm). The uranium content varies from 0.6 to 1.1 with an average value of 0.75 ppm (Table 1). Generally, the Pila Spi carbonate is highly depleted in trace elements compared with PAAS (Table 1 and Fig. 5).

Rare earth elements

The REEs belong to a coherent group of elements described by a similar ionic radius and trivalent oxidation state in most physiochemical conditions in the Earth's crust (Bau 1991). The ΣREE in the Pila Spi carbonate ranges from 3.86 to 9.98 ppm (Table 1). Within these, the LREE content ranges from 3.27 to 8.78 ppm and HREE content ranges from 0.53 to 1.22 ppm. The ΣREE shows a significant positive correlation with Al_2O_3, Fe_2O_3, P_2O_5, Y, and Co and negative correlation with Na_2O (Table 2). PAAS-normalized REE patterns of the studied carbonate exhibit seawater-like REE pattern with LREE depletion and HREE enrichment. The samples show negative Ce anomaly (Ce/Ce* = 0.91) and positive Eu anomaly (Eu/Eu* = 1.26) as shown in Fig. 6 and Table 3. The average $(Nd/Yb)_n$ ratio is 0.81, and the $(La/Yb)_n$ ratio ranges from 0.65 to 1.05 with an average value of 0.82. The $(Dy/Yb)_n$ ratio ranges from 1.00 to 1.42 with an average value of 1.18. The Y/Ho ratio of the Pila Spi carbonate varies from 25.00 to 36.67 with an average 30.07; the average of Er/Nd is 0.12 (Table 3).

Stable isotopes

The $\delta^{13}C$ values of whole carbonate samples are between −6.17 and 0.76‰ with an average −1.18‰, and the $\delta^{18}O$ values vary from − 3.85 to 0.46‰ with an average − 0.75‰ PDB (Table 4). The significant positive correlation was observed between $\delta^{13}C$ and $\delta^{18}O$ values ($r = 0.949$, $n = 14$), and MgO with both $\delta^{13}C$ and $\delta^{18}O$ (0.941 and 0.940, respectively). However, significant negative correlation was recorded between $\delta^{13}C$ and $\delta^{18}O$ with CaO (0.943 and 0.910, respectively).

Discussion

Elemental associations

The abundance of MgO among the major oxides proposes that the dominance of this oxide as compared with CaO suggests that the carbonate phase present in the Pila Spi Formation is mainly dolomite. It is confirmed by high dolomitization ratios (0.14–0.77; average = 0.65) of the studied carbonates computed according to Singh et al. (2013). The positive correlations between CaO and other oxides (TiO_2, Al_2O_3, SO_3, and P_2O_5) suggest that these oxides are genetically related and indicate same mode of their origin. CaO shows negative correlation with MgO and Na_2O due to the dolomitization process (Table 2).

The Sr content in the carbonate that is characterized by less variable may be influenced by high-temperature environment. Distribution of Sr could be affected by the presence of Ca, and this is confirmed by the positive correlation between the CaO and Sr (Table 2), and this suggested that the Sr is genetically related to the CaO. Low Sr concentrations could be related to the dolomitization process. No significant correlation between Sr and total REE content in the Pila Spi samples suggests that the loss of Sr during dolomitization was not related to significant loss of REEs.

Table 1 Major, trace and rare earth element concentrations for carbonates of Pila Spi Formation, High Folded Zone, Northern Iraq

Sample no.	Pila Spi formation															PAAS
	PH1	PH2	PH3	PH4	PH5	PH6	PH7	PH8	PH9	PB1	PB2	PB3	PB4	PB5	Average	
Major oxides																
SiO_2	2.23	2.82	12.90	15.40	6.95	5.85	5.68	13.29	7.24	6.12	8.83	8.07	8.56	8.17	7.36	62.40
TiO_2	0.012	0.027	0.017	0.010	0.008	0.017	0.015	0.008	0.022	0.013	0.017	0.012	0.017	0.013	0.015	0.99
Al_2O_3	0.75	1.73	1.04	0.46	0.58	0.98	0.92	0.4	1.27	0.87	1.1	0.69	0.98	0.75	0.9	18.90
Fe_2O_3	0.31	0.63	0.57	0.23	0.46	0.26	0.31	0.17	0.4	0.29	0.51	0.23	0.54	0.23	0.37	0.11
CaO	36.26	44.52	26.81	26.67	27.51	35.42	28.7	25.97	27.3	28.42	26.95	26.74	26.39	27.86	29.15	0.22
MgO	14.99	6.27	20.75	18.92	21	12.65	21.41	19.17	20.58	20.17	20.17	20.5	20.25	20.17	18.79	1.30
MnO	0.024	0.012	0.021	0.023	0.021	0.016	0.018	0.023	0.018	0.012	0.022	0.018	0.022	0.017	0.019	7.22
Na_2O	0.05	0.03	0.08	0.08	0.05	0.08	0.11	0.08	0.08	0.08	0.08	0.11	0.08	0.08	0.08	1.20
K_2O	0.02	0.07	0.05	0.02	0.02	0.05	0.05	0.02	0.10	0.05	0.05	0.05	0.05	0.05	0.05	3.70
SO_3	0.05	0.08	0.05	0.03	0.03	0.08	0.03	0.03	0.03	0.03	0.03	0.03	0.03	0.03	0.04	-
P_2O_5	0.018	0.023	0.014	0.005	0.009	0.014	0.005	0.005	0.005	0.005	0.014	0.005	0.014	0.005	0.010	0.16
LOI	43.32	43.11	36.55	36.48	42.54	43.24	42.86	39.21	42.54	42.86	42.12	42.54	42.35	42.44	42.51	-
Total	98.03	99.32	98.85	98.33	99.18	98.66	100.1	98.38	99.59	98.92	99.89	99.00	99.28	99.82	99.29	
Trace elements																
Rb	0.8	1.7	1.4	0.5	0.6	1.4	1.3	0.4	2.0	1.2	1.3	1.2	1.3	1.1	1.15	160
Sr	145	211	88.8	80.8	80.1	157	84.6	78.4	81.8	93.8	96.4	93.8	92.3	148	107.1	200
Th	0.2	0.4	0.2	0.2	0.2	0.2	0.2	0.2	0.2	0.2	0.2	0.2	0.2	0.2	0.21	
U	0.7	0.6	0.6	0.7	0.8	0.7	0.9	0.6	1.1	0.9	0.7	1	0.7	1	0.75	3.1
Y	2.1	1.8	2.1	1.1	2	1.1	1.2	1	1.8	1	2	1.1	1.8	1	1.4	27
Zr	2.3	5.6	2.3	1.3	2	3.3	2.9	1.1	3.3	4	2.3	2.1	2.5	2.1	2.6	210
Nb	0.6	1.0	0.5	0.4	0.4	0.7	0.5	0.3	0.6	0.4	0.5	0.4	0.4	0.5	0.45	1.90
Sc	0.5	1	0.7	0.4	0.4	0.6	0.7	0.3	0.9	0.7	0.9	0.6	0.8	0.6	0.65	16
V	13	23	13	15	28	13	16	14	9	15	16	14	13	19	15.7	150
Cr	12	32	13	13	9	10	8	14	10	9	13	7	13	9	11.82	110
Co	4.1	4.2	2.7	2.4	2.8	3.2	3.5	2.4	3.7	3	3.4	3.4	3.4	3.3	3.26	23
Ni	19.5	23.8	20.4	14.2	20.9	21.9	21.8	14.4	19.1	20.6	25.8	17.9	25.6	22.4	20.96	55
Cu	5	10.7	2.1	2.7	3.2	7.5	4	2.2	3.4	3.7	2.2	3	2.4	4.3	3.83	50
Zn	2	3	3	2	3	3	3	2	3	2	3	<2	3	2	2.55	85
Mo	0.23	0.24	0.22	0.26	0.45	0.34	0.57	0.29	0.45	0.31	0.22	0.81	0.17	0.2	0.34	1.5
Rare earth elements																
La	2.0	2.1	1.5	0.8	1.7	1.0	1.0	0.7	1.5	1.0	1.7	1.1	1.6	1.0	1.34	38.2
Ce	3.83	4.23	3.16	1.55	3.38	1.82	1.72	1.35	2.78	1.68	3.44	1.86	3.17	1.44	2.53	79.6
Pr	0.48	0.43	0.33	0.2	0.33	0.21	0.22	0.18	0.36	0.22	0.38	0.27	0.34	0.22	0.3	8.83
Nd	1.8	1.6	1.3	0.9	1.3	0.8	0.9	0.8	1.4	0.8	1.4	1.0	1.3	0.8	1.15	33.9
Sm	0.42	0.33	0.32	0.2	0.26	0.18	0.19	0.19	0.36	0.16	0.32	0.22	0.28	0.19	0.26	5.55
Eu	0.1	0.09	0.09	0.05	0.07	0.05	0.05	0.05	0.09	0.04	0.09	0.06	0.09	0.05	0.07	1.08
Gd	0.39	0.35	0.32	0.19	0.29	0.17	0.18	0.17	0.34	0.17	0.33	0.24	0.32	0.19	0.26	4.66
Tb	0.06	0.06	0.05	0.03	0.04	0.03	0.03	0.03	0.05	0.02	0.05	0.04	0.05	0.03	0.04	0.77
Dy	0.33	0.3	0.34	0.18	0.29	0.16	0.17	0.17	0.29	0.14	0.32	0.19	0.29	0.16	0.24	4.68
Ho	0.07	0.06	0.07	0.04	0.06	0.03	0.04	0.03	0.06	0.03	0.07	0.04	0.07	0.04	0.05	0.99
Er	0.18	0.19	0.2	0.1	0.18	0.09	0.1	0.09	0.17	0.08	0.2	0.11	0.19	0.09	0.14	2.85
Tm	0.03	0.03	0.03	0.01	0.03	0.01	0.01	0.01	0.02	0.01	0.03	0.01	0.03	0.01	0.02	0.41
Yb	0.14	0.18	0.17	0.08	0.15	0.09	0.09	0.08	0.15	0.07	0.18	0.09	0.17	0.08	0.12	2.82
Lu	0.02	0.03	0.03	0.01	0.02	0.02	0.01	0.01	0.02	0.01	0.03	0.02	0.03	0.01	0.02	0.43
ΣREE	9.85	9.98	7.91	4.34	8.1	4.66	4.71	3.86	7.59	4.43	8.54	5.25	7.93	4.31	6.53	184.77

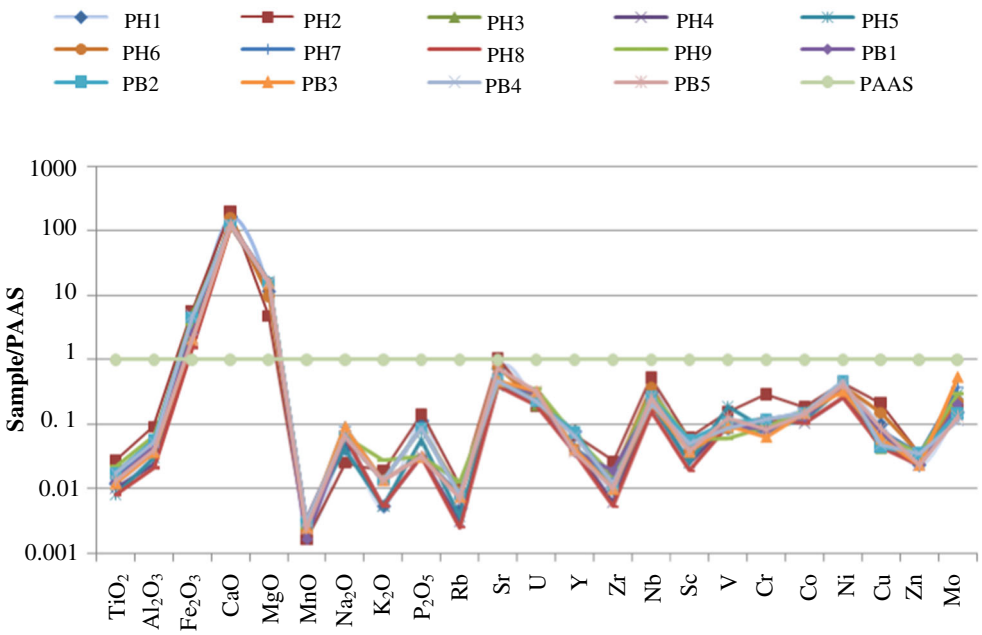

Fig. 5 Post-Archaean Australian Shale (PAAS)–normalized oxides and trace element patterns for the carbonates of Pila Spi Formation. PAAS values are from Taylor and McLennan (1985)

Zn shows positive correlation with the Fe_2O_3; this reflects its association with the iron oxide phases. Positive correlation was recorded between Rb and K_2O due to association and replacement in the clay minerals. The divalent cations such as Co and Cu could replace Ca^{2+} under suitable conditions during the deposition of the limestone (Reeder 1983), this supported by their positive correlation with the CaO (Table 2).

Sources of the rare earth elements

The REE contents in seawater are influenced by various input sources (detrital material from continental weathering and hydrothermal) and scavenging processes related to salinity, depth, and oxygen conditions (Greaves et al. 1999). The REE patterns of the sedimentary rocks could be utilized to characterize the source of these rocks (Armstrong-Altrin et al. 2015; Tobia 2018; Mitra et al. 2018; Roy et al. 2018; Ramos-Vázquez and Armstrong-Altrin 2019). Seawater REE patterns that are normalized to a PAAS are characterized by (1) consistent light REE depletion, (2) a negative Ce anomaly, (3) a slight positive La anomaly (Bau and Dulski 1996a, 1996b), and (4) high Y/Ho ratios (Bau 1996).

Ce/Ce* ratio is a function of a relative proportions of a pure seawater precipitate and clastic contamination, with increasing the clastics the ratio approaches to 1 (Madhavaraju and González-León 2012). In seawater, Ce/Ce* value ranges from less than 0.1 to 0.4 (Piepgras and Jacobsen 1992). The Ce/Ce* ratios from 0.71 to 1.04 (average = 0.91; Table 3) in the

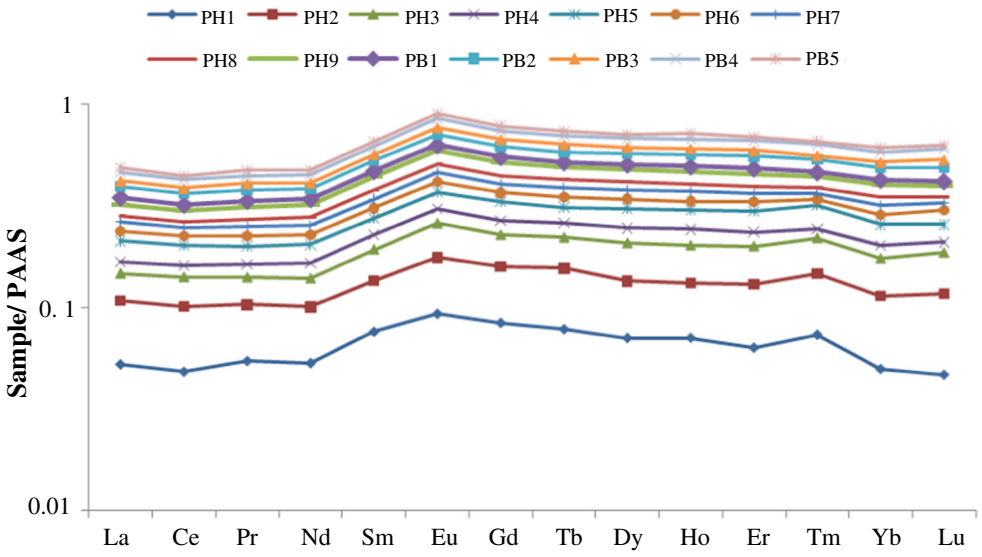

Fig. 6 PAAS normalized rare earth element patterns for the carbonates of the Pila Spi Formation. PAAS normalization values are from Taylor and McLennan (1985)

Table 2 Correlation coefficient matrix of major and trace elements for carbonates of Pila Spi Formation

	SiO_2	TiO_2	Al_2O_3	Fe_2O_3	CaO	MgO	MnO	Na_2O	K_2O	SO_3	P_2O_5	LOI	Rb
SiO_2	1												
TiO_2	− .415	1											
Al_2O_3	− .509	.978	1										
Fe_2O_3	− .177	.652	.722	1									
CaO	− .741	.567	.607	.293	1								
MgO	.553	− .548	− .553	− .251	− .957	1							
MnO	.495	− .516	− .561	− .083	− .461	.408	1						
Na_2O	.374	− .273	− .350	− .484	− .670	.661	.077	1					
K_2O	− .257	.827	.783	.371	.161	− .123	− .570	.102	1				
SO_3	− .500	.558	.561	.300	.864	− .892	− .397	− .509	.171	1			
P_2O_5	− .485	.562	.617	.689	.754	− .740	− .043	− .691	.060	.749	1		
LOI	− .957	.340	.422	.033	.641	− .489	− .532	− .250	.258	.419	.353	1	
Rb	− .398	.893	.874	.501	.298	− .229	− .569	.047	.952	.344	.279	.365	1
Sr	− .642	.543	.564	.212	.908	− .892	− .497	− .585	.197	.812	.685	.588	.312
Th	− .421	.666	.700	.507	.800	− .817	− .523	− .626	.308	.626	.617	.321	.347
U	− .137	− .029	− .046	− .353	− .336	.458	− .320	.463	.469	− .479	− .645	.217	.321
Y	− .196	.351	.424	.800	.195	− .104	.340	− .532	.115	.162	.650	.015	.248
Zr	− .696	.804	.860	.478	.729	− .649	− .830	− .398	.635	.606	.491	.645	.716
Nb	− .651	.816	.828	.459	.906	− .864	− .522	− .563	.493	.837	.714	.541	.605
Sc	− .383	.908	.924	.681	.329	− .268	− .493	− .096	.836	.263	.429	.344	.901
V	− .197	− .115	.017	.277	.266	− .215	− .198	− .521	− .293	.096	.185	.155	− .277
Cr	− .222	.620	.631	.564	.721	− .795	− .267	− .689	.180	.604	.705	.113	.224
Co	− .831	.655	.690	.351	.657	− .505	− .334	− .310	.508	.386	.545	.759	.609
Ni	− .483	.552	.635	.658	.273	− .176	− .294	− .187	.390	.239	.535	.492	.551
Cu	− .710	.596	.619	.208	.951	− .926	− .638	− .556	.280	.851	.597	.659	.376
Zn	− .151	.462	.488	.616	.204	− .171	− .010	− .375	.252	.295	.413	.088	.333
Mo	− .113	− .167	− .161	− .327	− .193	.266	− .176	.529	.146	− .227	− .467	.156	.093
∑REE	− .410	.501	.579	.808	.461	− .371	.142	− .669	.190	.325	.790	.235	.328

Table 2 (continued)

	Sr	Th	U	Y	Zr	Nb	Sc	V	Cr	Co	Ni	Cu	Zn	Mo
SiO_2														
TiO_2														
Al_2O_3														
Fe_2O_3														
CaO														
MgO														
MnO														
Na_2O														
K_2O														
SO_3														
P_2O_5														
LOI														
Rb														
Sr	1													
Th	.732	1												
U	− .234	− .322	1											
Y	.062	.181	− .308	1										
Zr	.639	.741	.032	.132	1									
Nb	.859	.800	− .178	.292	.799	1								
Sc	.338	.488	.135	.372	.736	.596	1							
V	.270	.435	− .140	.136	.161	.170	− .113	1						
Cr	.647	.931	− .574	.295	.577	.711	.421	.312	1					
Co	.627	.494	.201	.373	.638	.708	.650	− .013	.356	1				
Ni	.379	.264	− .036	.423	.500	.405	.712	.235	.209	.540	1			
Cu	.914	.801	− .179	− .005	.781	.908	.351	.314	.660	.594	.287	1		
Zn	.108	.193	− .335	.497	.323	.369	.393	.157	.301	.098	.515	.201	1	
Mo	− .300	− .163	.580	− .286	− .048	− .174	− .103	− .009	− .421	.057	− .274	− .096	− .510	1
∑REE	.333	.447	− .308	.936	.357	.512	.489	.206	.510	.602	.484	.266	.395	− .275

More than 0.660: Correlation is significant at the 0.01 level (2-tailed), 0.535 to 0.660: Correlation is significant at the 0.05 level (2-tailed)

Table 3 Elemental ratios and anomalies of the carbonate rocks of Pila Spi Formation

	PK1	PK2	PK3	PK4	PK5	PK6	PK7	PK8	PK9	PQ1	PQ2	PQ3	PQ4	PQ5	Average
Ce/Ce*	0.90	1.03	1.04	0.89	1.04	0.92	0.85	0.88	0.87	0.83	0.99	0.79	0.99	0.71	0.91
Eu/Eu*	1.16	1.25	1.32	1.21	1.20	1.35	1.27	1.31	1.21	1.14	1.30	1.23	1.42	1.24	1.26
(Nd/Yb)n	1.07	0.74	0.64	0.94	0.72	0.74	0.83	0.83	0.78	0.95	0.65	0.92	0.64	0.83	0.81
(La/Yb)n	1.05	0.86	0.65	0.74	0.84	0.82	0.82	0.65	0.74	1.05	0.70	0.90	0.69	0.92	0.82
(Dy/Yb)n	1.42	1.00	1.21	1.36	1.16	1.07	1.14	1.28	1.16	1.21	1.07	1.27	1.03	1.21	1.18
(Gd/Yb)n	1.69	1.18	1.14	1.44	1.17	1.14	1.21	1.29	1.37	1.47	1.11	1.61	1.14	1.44	1.31
Y/Ho	30.00	30.00	30.00	27.50	33.33	36.67	30.00	33.33	30.00	33.33	28.57	27.50	25.71	25.00	30.07
Er/Nd	0.10	0.12	0.15	0.11	0.14	0.11	0.11	0.11	0.12	0.10	0.14	0.11	0.15	0.11	0.12
Mg/Ca	0.21	0.07	0.40	0.36	0.39	0.18	0.38	0.38	0.39	0.36	0.38	0.39	0.39	0.37	0.33
Sr/Ca × 10^{-5}	16	18	13	12	11	17	11	12	12	13	14	14	14	21	14

studied carbonates (the samples are highly dolomitized) indicate that was precipitated from the seawater with some clastic input from the surrounding clastic continental materials. The Pila Spi carbonate samples have consistent seawater-like REE patterns (Fig. 6). The sensitivity to detrital contamination was explored by Nothdurft et al. (2004). The relatively high REE contents of the shale, even small amounts (e.g., 1–2%), greatly decreases the degree of LREE depletion and reduces the Ce and La anomalies. A negative Ce anomaly in oxygenated condition can be interpreted by oxidation of soluble Ce^{3+} to less soluble Ce^{4+} and consecutive removal by suspended particles with scavenging process results a negative Ce anomaly in seawater (Sholkovitz et al. 1994). Banner et al. (1988) found that dolomitization of the limestones had little effect on REE signatures, despite a high degree of diagenetic alteration. They suggest that where the rocks and diagenetic fluids have comparable REE distributions, the REE pattern will not be significantly changed by dolomitization.

Table 4 Carbon and oxygen isotopic data (as standard deviation with reference to V-PDB), of carbonate rocks from Pila Spi Formation (Kurdistan Region, Haibatt Sultan, and Bekhme sections)

Sample no.	CO_2	$\delta^{18}O_{VPDB}$	SD	$\delta^{13}C_{VPDB}$	SD
PH1	7482	− 1.36	0.11	− 3.29	0.09
PH2	7018	− 3.85	0.08	− 6.17	0.05
PH3	6892	− 0.55	0.08	− 0.97	0.06
PH4	6292	− 0.43	0.08	0.09	0.06
PH5	7792	− 0.70	0.08	0.11	0.05
PH6	7528	− 2.14	0.10	− 3.90	0.09
PH7	7504	0.07	0.09	0.25	0.05
PH8	6928	− 0.20	0.13	0.29	0.10
PH9	7005	0.46	0.08	− 0.21	0.06
PB1	7835	− 0.28	0.13	− 0.39	0.06
PB2	7008	− 0.56	0.10	− 1.06	0.09
PB3	6761	0.37	0.10	0.76	0.06
PB4	6045	− 0.72	0.11	− 0.92	0.08
PB5	7892	− 0.60	0.13	− 1.07	0.06
Average		− 0.75		− 1.18	

PH Haibat Sultan section, *PB* Bekhme section

The PAAS-normalized positive Eu anomaly is found either in waters affected by aeolian input (Elderfield 1988) or sediment provided through rivers, hydrothermal solutions, or from alteration of high-temperature basalt along mid-ocean ridges, back arc spreading center (German et al. 1993; Siby et al. 2008). The positive Eu anomaly (1.14–1.42, average = 1.26; Table 3) in the studied carbonates may be due to the suspended sediments derived through the rivers from the continent.

The average $(Nd/Yb)_n$ ratio of 0.81 in the studied carbonates is almost equal to the $(Nd/Yb)_n$ ratios of the carbonates of Arabian Sea (0.85 ± 0.17; Table 5). The $(Nd/Yb)_n$ ratio less than 1 represents depletion in LREE and proposes coastal/shallow marine origin of these carbonates (Srivastava and Singh 2019). The average $(La/Yb)_n$ ratio of 0.82 (Table 5) is less than the value suggested by Sholkovitz (1990) ($(La/Yb)_n$ = 1.3) and Condie (1991) ($(La/Yb)_n$ = 1) for terrigenous rocks. This could be due to the chemical and biochemical nature of the sediments (Srivastava and Singh 2019). Moreover, the range of $(Dy/Yb)_n$ ratio from 1.00 to 1.42 with an average value of 1.18 is nearly similar to the Arabian Sea carbonates ratio (1.12 ± 0.11; Table 5). The higher $(Dy/Yb)_n$ values represent enrichment of HREE than the LREE similar to the modern seawater (Nagarajan et al. 2011).

The super-chondritic Y/Ho ratio strongly depends on the salinity of the depositional environment, and it shows higher Y/Ho ratio (~ 44–74) for seawater than the estuaries and river water (Lawrence et al. 2006; Srivastava and Singh 2019). The volcanic ash and clastic materials have nearly constant chondritic Y/Ho ratio of ~ 28. In addition, the Y/Ho ratio of marine carbonates is higher than the freshwater carbonates (Webb and Kamber 2000; Shields and Webb 2004). Low to fairly comparable values of Y/Ho ratios (25.00–36.67; average = 30.07) in the studied carbonates (Table 3) suggest influence of fresh water input from the rivers to the seawater that lower this ratio

Table 5 Geochemical comparison of the carbonates of Pila Spi Formation with that of Arabian sea and shallow marine carbonates

Elements ratio	Pila Spi carbonates[a]	Arabian sea carbonates[b]	Shallow marine carbonates[c]
Ce/Ce*	0.91	0.84 ± 0.06	0.76 ± 0.16
Eu/Eu*	1.26	1.15 ± 0.08	0.58 ± 0.11
$(La/Yb)_n$	0.82	0.85 ± 0.2	1.82 ± 0.46
$(Nd/Yb)_n$	0.81	0.85 ± 0.17	1.51 ± 0.30
$(Dy/Yb)_n$	1.18	1.12 ± 0.11	1.25 ± 0.17
(Y/Ho)	30.07	34.14 ± 1.64	-
Er/Nd	0.12	0.11 ± 0.02	0.07 ± 0.02
ΣREE	6.53	78 ± 40	73 ± 20

[a] Present study

[b] Nath et al. (1997)

[c] Madhavaraju and Ramasamy (1999)

during the precipitation (Srivastava and Singh 2018). However, Y/Ho ratios appear to decrease with increasing dolomite content (Nothdurft et al. 2004), similar less consistent trend of decreasing LREE depletion $(Nd/Yb)_n$ occurs with increasing dolomite content, and the negative Ce anomaly is absent in some dolomitized samples.

Er/Nd ratio can be a representative of the influence of LREE/HREE fractionation in the marine conditions (German and Elderfield 1989). The higher Er/Nd ratio value was recorded for the marine carbonate (near 0.27; De Baar et al. 1988). Er/Nd ratio less than 0.1 indicates addition of detrital material as well as diagenetic process within the carbonates (De Baar et al. 1988; Tobia 2018). Er/Nd ratios of the Pila Spi carbonate samples are within 0.10 to 0.14 with an average of 0.12 (Table 3) which is lower than that of the normal marine water. This confirms the influence of terrigenous input on the carbonate during the sedimentation.

The negative Ce anomaly reflects the combination of REE from seawater or from the pore water under oxic condition, and mixing with terrigenous materials in the marine sediments. The terrigenous input in these carbonate is confirmed by significant positive correlation of ΣREE with Al_2O_3 (0.579, n = 14), and significant positive correlation of TiO_2 with Cr and Sc (0.620 and 0.908, respectively) (Hernandez-Hinojosa et al. 2018).

Dipositional environment

The Pila Spi carbonates have different degree of diagenetic effects; the most abundance of them is dolomitization. According to the crystal size and crystal boundary shape, the fabric of dolomite was classified to three microfacies (unimodal fine crystalline planar-e to planar-s, unimodal fine crystalline planar-s to non-planar-a, and bimodal fine to medium crystalline planar-s to non-planar-a dolomite). Silicification of late diagenetic stage is common feature in the studied carbonate. Also, blocky calcite cement of late diagenetic was recorded.

The sediments deposited in oxygenated environment are characterized by low contents of U (Madhavaraju and Ramasamy 1999), whereas high U contents are recorded in sediments from the oxygen-poor zones (Nath et al. 1997). In addition, the uranium is mobilized as U^{+6} in oxic condition and precipitates as U^{+4} in reducing environments (Wright et al. 1984; Madhavaraju and González-León 2012). The low U content (0.60–1.10; average = 0.75 ppm) in the studied carbonates (Table 1) suggests that the Pila Spi carbonates were precipitated under oxic environments.

REE patterns may contain redox sensitive Ce anomalies; Ce is unique among the REE because it can exist in both the +3 and +4 oxidation state. In the presence of oxygen, Ce^{3+} is partially oxidized to Ce^{4+} on the surface of Mn (oxyhydr) oxides, where it no longer participates in solid-solution exchange reactions, leaving residual seawater depleted in Ce relative to other trivalent REEs (German and Elderfield 1990). This fractionation of Ce only occurs under oxic conditions (German et al. 1991). The marine well oxygenated conditions may prefer the scavenging of Ce(OH) on the Fe-Mg coating the particles. The Ce/Ce* values in the studied carbonates have positive correlation with scavenging-type particle reactive element (Fe, r = 0.804, n = 14) which indicates that the variations in Ce anomalies might be related to scavenging processes (Masuzawa and Koyama 1989).

The $\delta^{18}O$ signatures of the dolomitizing fluids are derived due to evaporation or through water-rock interactions. The oxygen isotopic composition of the dolomites was probably the result of fluid evaporation (Gill et al. 1995). The dolomites become depleted in both ^{13}C and ^{18}O and in transects from the modern phreatic zone in the center to the vadose zone at the margins. The dominant observation of the blocky calcite cements with clear twining in the carbonate of Pila Spi Formation is a good evidence for the phreatic conditions (Fig. 4h). The trend may be controlled by meteoric recrystallization, chemical gradients during dolomitization, or both. Dolomitization was probably due to the mixing of seawater and due to evaporation to produce a fluid with an oxygen

isotopic composition enriched in ^{18}O relative to normal seawater. The dolomitized beds occur within a lagoon that was in a freshwater discharge area and could allow extensive evaporation to take place.

The $\delta^{13}C$ and $\delta^{18}O$ values of carbonate rocks can be employed to discriminate whether the basin was open or closed and to predict the paleo-salinity of the sedimentary environment (Talbot 1990). In open freshwater basins, the water stays for a short time, and the carbon and oxygen isotopic values are both negative, and there is no clear correlation between them. However, in a closed saltwater environment, the water is invariant, and the $\delta^{13}C$ and $\delta^{18}O$ values of the carbonate rocks have a significant correlation (Fig. 7). The strongly the closed system, the higher the correlation coefficient. The correlation coefficient (r) of the $\delta^{13}C$ and $\delta^{18}O$ in the carbonate of Pila Spi Formation is 0.949 (n = 14), indicating significant strong correlation (Wang et al. 2014) and closed system. Both $\delta^{13}C$ and $\delta^{18}O$ values are related to salinity, and the variation trend is that the higher the salinity corresponded to the higher δ value.

Conclusions

1. The Pila Spi carbonate possesses low ΣREE contents, fairly high Y/Ho ratios, low $(Nd/Yb)_n$ ratios, and seawater-like REE patterns suggesting that the REE concentrations were mainly derived from seawater.
2. The positive correlations of Al_2O_3 with ΣREE contents, Er/Nd ratios, and positive Eu anomaly suggest that some terrigenous sediments were incorporated in these carbonates.
3. The low concentrations of Uranium and negative Ce anomaly suggest oxic condition of deposition for the Middle–Late Eocene Pila Spi carbonate.
4. The lower to slightly comparable values of Y/Ho ratio (19.54- 48.75) in the studied carbonates suggest input of freshwater into the seawater during precipitation of these carbonates.
5. The positive covariance between $\delta^{13}C$ and $\delta^{18}O$ indicates the early diagenetic alteration of carbonates in the marine meteoric mixing zone.
6. Geochemical comparable of the Pila Spi carbonate with that of Arabian sea carbonate suggests that the basin had identical chemical characteristics with that of the Arabian Sea.

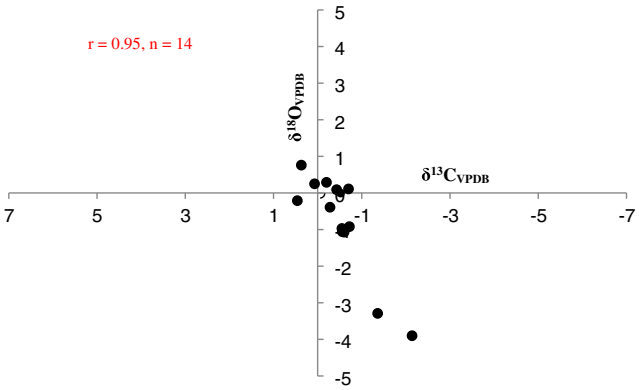

Fig. 7 Bivariate plots of $\delta^{18}O$ (V-PDB) and $\delta^{13}C$ (V-PDB) for the Pila Spi carbonates

Acknowledgments The authors would like to thank Dr. Mohamad Fakhre, Salahaddin University, Department of Geology, for his help in the petrographic section. We are thankful to an anonymous reviewers for their valuable suggestions and kind help in improving the quality of the manuscript.

References

Alexander BW, Bau M, Andersson P, Dulski P (2008) Continentally-derived solutes in shallow Archean seawater: rare earth element and Nd isotope evidence in iron formation from the 2.9 Ga Pongola Supergroup, South Africa. Geochim Cosmochim Acta 72: 378–394

Al-Mashaikie SZ, Latif RM (2017) Sedimentology and lithostratigraphy of the Pila Spi Formation in Koi Sanjaq area, NE Iraq: new insight for depositional environment and basin configuration. Iraqi J Sci 58: 669–686

Al-Qayim B, Al-Shaibani S (1997) Lithostratigraphy of Cretaceous–Tertiary transect Bekhme Gorge, NE Iraq. Iraqi Geol J 28(2):127–136

Al-Qayim B, Al-Shaibani S, Nisan B (1988) Stratigraphic evolution of Paleogene sequence Haibat Sultan, Northeastern Iraq. J Geol Soc Iraq 21(2):51–61

Al-Qayim B, Al-Shaibani S, Nissan B (1994) A bimodal tidal depositional system of the Gercus Formation, Shaqlawa area, Northern Iraq. Iraqi Geol J 27(2):75–95

Al-Sakry SI (1999) Stratigraphy and facies of Paleogene carbonate formations of selected sections, Northeastern Iraq. M Sc Thesis, University of Baghdad

Armstrong-Altrin JS, Verma SP, Madhavaraju J, Lee YI, Ramasamy S (2003) Geochemistry of Late Miocene Kudankulam Limestones, South India. Int Geol Rev 45:16–26

Armstrong-Altrin JS, Madhavaraju J, Sial AN, Kasper-Zubillaga JJ, Nagarajan R, Flores-Castro K, Rodríguez JL (2011) Petrography and stable isotope geochemistry of the Cretaceous El Abra Limestones (Actopan), Mexico: implication on diagenesis. J Geol Soc India 77:349–359

Armstrong-Altrin JS, Machain-Castillo ML, Rosales-Hoz L, Carranza-Edwards A, Sanchez-Cabeza JA, Ruíz-Fernández AC (2015) Provenance and depositional history of continental slope sediments in the Southwestern Gulf of Mexico unraveled by geochemical analysis. Cont Shelf Res 95:15–26

Banner JL, Hanson GN, Meyers WJ (1988) Water-rock interaction history of regionally extensive dolomites of the Burlington- Keokuk Formation (Mississippian): isotopic evidence. In: Shukla V, Baker P (eds) Sedimentology and geochemistry of dolostones. SEPM Special Publication 43. SEPM, Tulsa, pp 97–114

Bau M (1991) Rare-earth element mobility during hydrothermal and metamorphic fluid-rock interaction and the significance of the oxidation state of europium. Chem Geol 93:219–230

Bau M, Dulski P (1996a) Anthropogenic origin of positive gadolinium anomalies in river waters. Earth Planet Sci Lett 143:245–255

Bau M, Dulski P (1996b) Distribution of Y and rare-earth elements in the Penge and Kuruman Iron Formations, Traansvaal Supergroup, South Africa. Precambrian Res 79:37–55

Bellen RC, Dunnington HV, Wetzel R, Morton D (1959) Lexique Stratigraphic International. Asie, Fasc. 10a, Iraq, Paris

Choquette PW, Pray LC (1970) Geologic nomenclature and classification of porosity in sedimentary carbonates. Bull Am Assoc Pet Geol 54: 207–250

Condie KC (1991) Another look at rare earth elements in shales. Geochim Cosmochim Acta 55:2527–2531

Cuna S, Pop D, Hosu A (2001) Carbon and oxygen isotope ratios in Rona limestone, Romania. Studia Universitatis Babeş-Bolyai, Geologia, XLVI, 1

De Baar HJW, German CR, Elderfield H, Van Gaans P (1988) Rare earth element distributions in anoxic waters of the Cariaco Trench. Geochim Cosmochim Acta 52:1203–1219

Deepulal PM, Kumar TR, Sujatha CH (2012) Behavior of REEs in a tropical estuary and adjacent continental shelf of southwest coast of India: evidence from anomalies. J Earth Syst Sci 121:1215–1227

Dickson JAD (1965) A modified staining technique for carbonates in thin section. Nature 205:587

Ditmar V Iraqi-Soviet Team (1971) Geological conditions and hydrocarbon prospects of the Republic of Iraq (Northern and Central parts). Manuscript report, INOC Library, Baghdad

Elderfield H (1988) The oceanic chemistry of the rare-earth elements. Phil Trans R Soc London 325:105–126

Elderfield H, Pagett R (1986) Rare earth elements in icthyoliths: variations with redox conditions and depositional environments. Sci Total Environ 49:175–197

Elderfield H, Upstill-Goddard R, Sholkovitz ER (1990) The rare-earth elements in rivers, estuaries, and coastal seas and their significance to the composition of ocean waters. Geochim Cosmochim Acta 54: 971–991

Fu XG, Wang J, Zeng YH, Tan F, He J (2011) Geochemistry and origin of rare earth elements (REEs) in the Shengli River oil shale, northern Tibet, China. Chem Erde 71:21–30

German CR, Elderfield H (1989) Rare earth elements in Saanich Inlet, British Columbia, a seasonally anoxic basin. Geochim Cosmochim Acta 53:2561–2571

German CR, Elderfield H (1990) Application of the Ce anomaly as a paleoredox indicator: the ground rules. Paleoceanography 5:823–833

German CR, Holliday BP, Elderfield H (1991) Redox cycling of rare earth elements in the suboxic zone of the black Sea. Geochim Cosmochim Acta 55:3553–3588

German CR, Higgs NC, Thomson J, Mills R, Elderfield H, Blusztajn J, Fleer AP, Bacon MP (1993) A geochemical study of metalliferous sediment from the TAG hydrothermal mound, 26°08′ N, Mid-Atlantic Ridge. J Geophys Res 98:9683–9692

Gill IP, Moore CH, Aharon P (1995) Evaporitic mixed-water dolomitization on St. Croix, U.S.V.I. J Sed Res 65:591–604

Greaves MJ, Elderfield H, Sholkovitz ER (1999) Aeolian sources of rare earth elements to the Western Pacific Ocean. Mar Chem 68:31–38

Gregg JM, Sibley DF (1984) Epigenetic dolomitization, and the origin of xenotropic dolomite texture. J Sediment Petrol 54(3):908–931

Hernandez-Hinojosa V, Montiel-Garcia PC, Armstrong-Altrin JS, Nagarajan R, Kasper-Zubillaga JJ (2018) Textural and geochemical characteristics of beach sands along the western Gulf of Mexico, Mexico. Carpathian J Earth Environ Sci 13(1):161–174

Hua G, Yuansheng D, Lian Z et al (2013) Trace and rare earth elemental geochemistry of carbonate succession in the Middle Gaoyuzhuang Formation, Pingquan Section: implications for Early Mesoproterozoic ocean redox conditions. J Palaeogeogr 2:209–221

Jassim SZ, Goff JC (2006) Geology of Iraq. Publishers Dolin and Moravian Museum, Prague

Jones B, Manning DAC (1994) Composition of geochemical indices used for the interpretation of paleoredox conditions in ancient mudstones. Chem Geol 111:111–129

Kadhim LS, Hussein SA (2016) Petrography and geochemistry of Pila Spi Formation (Middle- Late Eocene) in Selected Sections / Northern Iraq. Iraqi J Sci 57:2291–2306

Kato Y, Nakao K, Isozaki Y (2002) Geochemistry of Late Permian Triassic pelagic cherts from southwest Japan: implications for an oceanic redox change. Chem Geol 182:15–34

Khanaqa PA (2011) Interpretation of new facies in the Pila Spi Formation (Middle – Late Eocene) in Sulaimanyia NE Iraq. Iraqi Bull Geol Min 7(3):33–45

Lawrence MG, Greig A, Collerson KD, Kamber BS (2006) Rare earth element and yttrium variability in south east Queensland waterways. Aquat Geochem 12:39–72

Liu YG, Miah MRU, Schmitt RA (1988) Cerium: a chemical tracer for paleo-oceanic redox condition. Geochim Cosmochim Acta 52: 1361–1371

Lonoy A (2006) Making sense of carbonate system. AAPG 90(9):1381–1405

Lucia FJ (2007) Carbonate Reservoir Characterization: an integrated approach, 2nd edition. Springer Verlag, New York

Madhavaraju J, González-León CM (2012) Depositional conditions and source of rare earth elements in carbonate strata of the Aptian-Albian Mural Formation, Pitaycachi section, northeastern Sonora, Mexico. Revista Mexicana de Ciencias Geológicas 29(2):478–491

Madhavaraju J, Ramasamy S (1999) Rare earth elements in limestones of Kallankurichchi Formation of Ariyalur Group, Tiruchirapalli Cretaceous, Tamil Nadu. J Geol Soc India 54:291–301

Madhavaraju J, González-León CM, Lee YI, Armstrong-Altrin JS, Reyes-Campero LM (2010) Geochemistry of the Mural Formation (Aptian-Albian) of the Bisbee Group, Northern Sonora, Mexico. Cretac Res 31:400–414

Major RP, Vander Stoep GW, Holtz MH (1990) Delineation of unrecovered mobile oil in a mature dolomite reservoir: East Penwell San Andres Unit, University Lands, West Texas. The University of Texas at Austin, Bureau of Economic Geology, Report of Investigations No. 194, 52 pp

Masuzawa T, Koyama M (1989) Settling particles with positive Ce anomalies from the Japan Sea. Geophys Res Lett 16:503–506

Matilainen R, Tummavuori J (1999) Determination of SiO_2 in lime mud by gravimetry. Fresenius J Anal Chem 364:700–704

Mitra R, Chakrabarti G, Shome D (2018) Geochemistry of the Palaeo-Mesoproterozoic Tadpatri shales, Cuddapah Basin, India: implications on provenance, paleoweathering and paleoredox conditions. Acta Geochem 37:715–733

Morad S, Al-Aasm IS, Sirat M, Sattar MM (2010) Vein calcite in Cretaceous carbonate reservoirs of Abu Dhabi: record of origin of fluids and diagenetic conditions. J Geochem Explor 106:156–170

Murray RW, Buchholtz MR, Brumsack HJ (1991) Rare earth elements in Japan Sea sediments and diagenetic behavior of Ce/Ce*, results from ODP leg 127. Geochim Cosmochim Acta 55:2453–2466

Murray RW, Buchholtz MR, Gerlach DC et al (1992) Interoceanic variation in the rare earth, major and trace element depositional chemistry of chert: perspectives gained from the DSDP and ODP record. Geochim Cosmochim Acta 56:1897–1913

Nagarajan R, Madhavaraju J, Armstron-Altrin JS, Nagendra R (2011) Geochemistry of Neoproterozoic limestones of the Shahabad Formation, Bhima Basin, Karnataka, southern India. Geosci J 15: 9–25

Nath BN, Bau M, Ramalingeswara RB, Rao CM (1997) Trace and rare earth elemental variation in Arabian Sea sediments through a transect across the oxygen minimum zone. Geochim Cosmochim Acta 61:2375–2388

Nothdurft LD, Webb GE, Kamber BS (2004) Rare earth element geochemistry of Late Devonian reefal carbonates, canning basin, Western Australia: confirmation of a seawater REE proxy in ancient limestones. Geochim Cosmochim Acta 68(2):263–283

Othman DH, Al-Qayim BA (2010) Lithofacies association, dolomitization, and potentiality of the Pila Spi formation, Taq Taq oil field, NE Iraq. Iraqi Bull Geol Min 6(2):95–114

Patra A, Singh PB (2017) Geochemistry of the Eocene limestones of the Jaisalmer Basin, Rajasthan, India: implications on depositional conditions and sources of rare earth elements. Geochem Int 55:1180–1192

Pattan JN, Masuzawa T, Borole DV, Parthiban G, Jauhari P, Yamamoto M (2005) Biological productivity, terrigenous influence and noncrustal elements supply to the central Indian Ocean Basin: paleoceanography during the past 1 Ma. J Earth Syst Sci 114:63–74

Piepgras DJ, Jacobsen SB (1992) The behaviour of rare earth elements in seawater: precise determination of ferromanganese crusts. Geochim Cosmochim Acta 56:851–1862

Piper DZ (1974) Rare earth elements in the sedimentary cycle, a summary. Chem Geol 14:285–304

Ramos-Vázquez MA, Armstrong-Altrin JS (2019) Sediment chemistry and detrital zircon record in the Bosque and Paseo del Mar coastal areas from the southwestern Gulf of Mexico. Mar Pet Geol 110: 250–275

Randazzo AF, Zachos LG (1984) Classification and description of dolomitic fabrics of rocks from the Floridan aquifer, USA. Sed Geol 37: 151–162

Reeder RJ (1983) Crystal chemistry of the rhombohedral carbonates. Min Soc Am Rev 11:1–48

Roy A, Chakrabarti G, Shome D (2018) Geochemistry of the Neoproterozoic Narji limestone, Cuddapah Basin, Andhra Pradesh, India: implication on palaeoenvironment. Arab J Geosci. https://doi.org/10.1007/s12517-018-4135-9

Schieber J (1988) Redistributionof rare earth elements during diagenesis of carbonate rocks from Mid-Proterozoic Newland Formation, Montana, USA. Chem Geol 69:111–126

Shields GA, Webb GE (2004) Has the REE composition of seawater changed over geologic time. Chem Geol 204:103–107

Sholkovitz ER (1990) Rare earth elements in marine sediments and geochemical standards. Chem Geol 88:333–347

Sholkovitz ER, Landing WM, Lewis BL (1994) Ocean particle chemistry: the fractionation of the rare earth elements between suspended particles and seawater. Geochim Cosmochim Acta 58:1567–1580

Sibley DF, Gregg JM (1987) Classification of dolomite rock textures. J Sediment Petrol 57:967–975

Siby K, Nath BN, Ramaswamy V et al (2008) Possible detrital, diagenetic and hydrothermal sources for Holocene sediments of the Andaman back arc basin. Mar Geol 247:178–193

Singh BP, Pawar JS, Patra A (2013) Geochemistry of Late Eocene/Oligocene calcretes (caliche) of the northwestern Himalaya, India. J Him Earth Sci 34(2):135–140

Sissakian VK (1997) Geological map of Arbeel and Mahabad Quadrangles, Sheets NJ-38-14 and NJ-38-15, scale 1: 250000, GEOSURV, Baghdad, Iraq

Sissakian VK (2000) Geological map of Iraq, sheet no.1, scale 1: 1000 000, 3rd ed. GEOSURV, Baghdad, Iraq

Srivastava VK, Singh BP (2017) Shoreface to estuarine sedimentation in the late Paleocene Matanomadh Formation, Kachchh, Western India. J. Asian Earth Sci 136:1–15

Srivastava VK, Singh BP (2018) Depositional environments and sources for the middle Eocene Fulra Limestone Formation, Kachchh Basin, western India: evidences from facies analysis, mineralogy, and geochemistry. Geol J 54:62–82. https://doi.org/10.1002/gj.3154

Srivastava VK, Singh BP (2019) Depositional environments and sources for the middle Eocene Fulra limestone Formation, Kachchh Basin, western India: evidences from facies analysis, mineralogy, and geochemistry. Geol J 54:62–82

Talbot MR (1990) A review of the palaeohydrological interpretation of carbon and oxygen isotopic ratios in primary lacustrine carbonates. Chem Geol Isot Geosci 80:26l–279l

Tandon SK, Andrews JE (2001) Lithofacies association and stable isotopes of palustrine and calcrete carbonates: examples from an Indian Maastrichtian regolith. Sedimentology 48:339–355

Tanner LH (2009) Continental carbonates as indicators of paleoclimate. In: Alonso-Zarza AM, Tanner L (eds) Carbonates in continental settings, developments in sedimentology 62, pp 179–214

Taylor SR, McLennan SM (1985) The continental crust: its composition and evolution. Blackwell Scientific Publications, Oxford

Tobia FH (2018) Stable isotope and rare earth element geochemistry of the Baluti carbonates (Upper Triassic), Northern Iraq. Geosci J 22: 975–987

Tobia FH, Shangola SS (2016) Mineralogy, geochemistry, and depositional environment of the Beduh shale (lower Triassic), Northern Thrust Zone, Iraq. Turk J Earth Sci 25:367–391

Toyoda K, Nakamura Y, Masuda A (1990) Rare earth elements of Pacific pelagic sediments. Geochim Cosmochim Acta 54:1093–1103

Wang BS, Lee CP, Ho TY (2014) Trace metal determination in natural waters by automated solid phase extraction system and ICP-MS: the influence of low level Mg and Ca. Talanta 128:337–344. https://doi.org/10.1016/j.talanta.2014.04.077

Webb GE, Kamber BS (2000) Rare earth elements in Holocene reefal microbialites: a shallow seawater proxy. Geochim Cosmochim Acta 64:1557–1565

Wright J, Seymour RS, Shaw HF (1984) REE and neodymium isotopes in conodont apatite variation with geological age and depositional environment. Geol Soc Am Spec Publ 196:325–340